Coaxial MnO₂/Carbon Nanotube Array Electrodes for High-Performance Lithium Batteries

Arava Leela Mohana Reddy,[†] Manikoth M. Shaijumon,[†] Sanketh R. Gowda,[‡] and Pulickel M. Ajayan*,[†]

Department of Mechanical Engineering & Materials Science, and Department of Chemical & Biomolecular Engineering, Rice University, 6100 Main Street, Houston, Texas 77005

ABSTRACT

Coaxial manganese oxide/carbon nanotube (CNT) arrays deposited inside porous alumina templates were used as cathodes in a lithium battery. Excellent cyclic stability and capacity of MnO₂/CNT coaxial nanotube electrodes resulted from the hybrid nature of the electrodes with improved electronic conductivity and dual mechanism of lithium storage. The reversible capacity of the battery was increased by an order compared to template grown MnO₂ nanotubes, making them suitable electrodes for advanced Li ion batteries.

A nanoscale approach to electrochemical energy storage applications such as in lithium batteries and supercapacitors has been of great interest because of their unique properties leading to improved performances.[1−5] Innovative materials chemistry has been the key to various advancements in lithium rechargeable batteries.[6,7] Various transition metal oxides have been widely studied as electrode materials for rechargeable lithium-ion batteries because of their high theoretical capacity, safety, environmental benignity, and low cost.[8−15] However, poor electronic conductivity of metal oxides limits them from use in high-performance lithium ion batteries. One of the other challenging issues is to tackle their capacity decay with cycling, leading from large volume expansion during the lithium uptake/release process. Extensive research efforts are presently devoted to overcome these problems by using electronically conductive additives and carbon coatings.[16−19] Among transition metal oxides, manganese oxide (MnO₂) has been studied as an electrode for lithium batteries with a high storage capacity, in addition to its low cost, environmental friendliness, and natural abundance.[20−23] However its potential applications in practical Li-ion batteries are limited due to its poor electrical conductivity and large volume expansion during repeated lithium cycling processes.[21] One-dimensional (1D) nanostructured morphologies of these electrodes with controlled size, crystallinity, and chemical composition have been designed to overcome some of these challenges.[24,25] However,

conductivity of these 1D nanowires remains an existing issue. Coaxial 1D nanowires of tin oxide core and indium oxide shell nanostructures have been shown to be promising Li-ion battery electrodes.[26] Coaxial nanowires/nanotubes will lead to multiple functionalities by combining the physical properties of different materials. In order to build Li batteries with improved capacity and power capabilities, coaxial nanowires/nanotubes of multiple materials with specific electrochemical and physicochemical properties need to be fabricated. Here, we demonstrate the fabrication of hybrid coaxial nanotubes of MnO₂ and carbon nanotubes (CNTs) as high-performance electrodes of lithium batteries. CNTs due to their outstanding electrical properties apart from their high chemical stability, high aspect ratio, strong mechanical strength, and high activated surface area, are attractive electrode materials in energy storage devices, such as electrochemical capacitors, fuel cells, and lithium batteries.[27−33] Careful engineering of hybrid coaxial electrode material having both high storage capacity metal oxide and highly conducting CNTs will lead to enhanced Li storage properties. The tubular morphology offers a unique combination of high porosity and low internal resistance. The work is aimed to increase the electronic conductivity and lithium storage capacity of MnO₂ nanotubes by using the coaxial nanotubes with MnO₂ nanotubes in the outer shell and highly conducting CNT in the inner core. The coaxial electrode configuration will have (i) improved electronic conductivity due to the presence of CNT, (ii) homogeneous electrochemical accessibility and high ionic conductivity by avoiding agglomerative binder and other conductive additives, (iii)

* To whom correspondence should be addressed, ajayan@rice.edu.
† Department of Mechanical Engineering & Materials Science.
‡ Department of Chemical & Biomolecular Engineering.

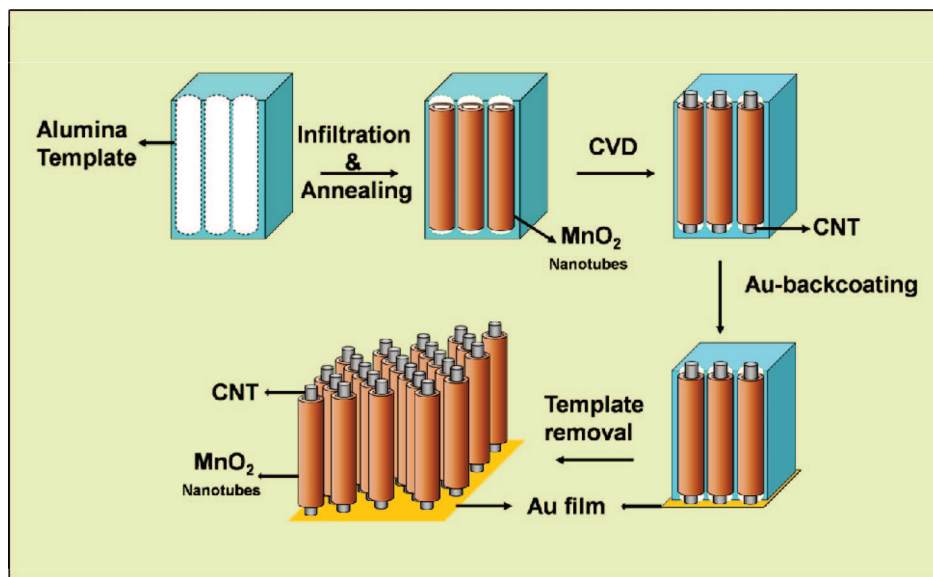**Figure 1.** Schematic diagram showing the fabrication of MnO_2/CNT hybrid coaxial nanotube arrays inside AAO template using a combination of simple vacuum infiltration and chemical vapor deposition techniques. A thin layer of gold (~100 nm) was sputter coated to act as current collector for the electrodes.
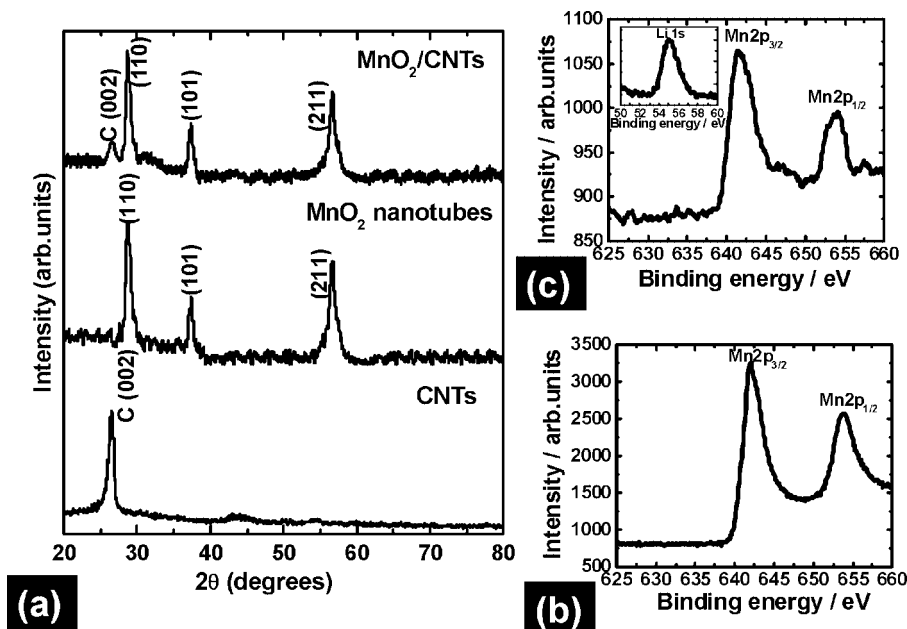

Figure 2. (a) X-ray diffraction patterns of MnO_2/CNT coaxial nanotubes, MnO_2 nanotubes, and CNTs. XPS spectra of MnO_2/CNT coaxial nanotubes (b) before and after (c) first lithium discharge process. Formation of manganese metal and Li_2O during the initial lithiation process has been confirmed using XPS.

well-directed 1D conductive paths due to perfect coaxial alignment, and (iv) a dual lithium storage mechanism (insertion/deinsertion in the case of CNTs and formation and decomposition of Li_2O in the case of MnO_2 nanotubes).

The coaxial nanotube structures have been prepared by a combination of simple vacuum infiltration and chemical vapor deposition techniques through a template approach (Figure 1). MnO_2 nanotubes are first fabricated by vacuum infiltration inside the channels of commercially available AAO templates (nanopore diameter of ~200 nm and length of ~50 μm), which is followed by the growth of CNTs using
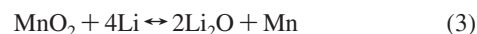
chemical vapor deposition (see Supporting Information for method and synthesis, section 1S). The sample was plasma etched for 30 min to remove the amorphous carbon layer that forms during chemical vapor deposition. A layer of Au film (~100 nm) was sputtered onto one side of the template which serves as the current collector for the electrode. The MnO_2/CNT hybrid coaxial structures are then released from the alumina templates by dissolving the templates in 3 M NaOH solution for 1 h. The presence of Au film holds the coaxial hybrid structures from collapsing, after the removal of templates. The morphology of the prepared MnO_2/CNT

coaxial nanotubes was characterized by scanning electron microscopy (FEI Quanta 400 ESEM FEG) and energy-dispersive X-ray spectroscopy (EDX). The powder X-ray diffraction patterns were obtained by a Rigaku D/Max Ultima II using Cu Kα radiation. For the X-ray photoelectron spectroscopy (XPS) analysis, PHI Quantera XPS was used. Flexible films of MnO_2/CNT coaxial nanotubes obtained after the removal of templates were directly used as electrode in the lithium battery. Electrochemical measurements were performed in a Swagelok-type cell using AUTOLAB PG-STAT 302N potentiostat/galvanostat (see Supporting Information for details, section 2S). An electrochemical test cell was assembled in argon-filled glovebox using the active material (MnO_2/CNT coaxial nanotubes) as working electrode, lithium metal foil as the counter/reference electrode, and 1 M solution of $LiPF_6$ in 1:1 (v/v) mixture of ethylene carbonate (EC) and dimethyl carbonate (DMC) as electrolyte. A glass microfiber filter was used as separator. The cells were charged and discharged galvanostatically at a rate of 50 mA/g between 3.2 and 0.2 V vs Li/Li^+.

The crystallinity of the coaxial nanotubes was confirmed by X-ray diffraction (XRD). XRD patterns of the MnO_2/CNT coaxial nanotubes show three well-resolved peaks that can be indexed as (100), (110), and (211) reflections associated with tetragonal symmetry (Figure 2a). An additional peak at 26.4° attributed to the (002) plane of hexagonal graphite structure, indicates the presence of CNTs. XRD patterns taken from MnO_2 nanotubes and CNTs are in good agreement with the reported literature (PDF#01-071-4824(RDB)). Elemental analysis by energy dispersive X-ray spectroscopy (EDX) revealed the presence of Mn and O (see Supporting Information, Figure 1S). The additional reflections of Al and Au in the EDX spectra are due to AAO template and gold back coating, respectively. MnO_2/CNT coaxial nanotubes before and after Li storage were characterized by X-ray photoelectron spectroscopy (XPS). XPS profiles of MnO_2/CNT hybrid coaxial nanotubes before Li storage (Figure 2b) and after Li storage (Figure 2c) are analyzed by focusing on the regions where the signals of Mn $2p_{3/2}$, Mn $2p_{1/2}$, C 1s, and Li 1s are expected. The peaks of Mn $2p_{3/2}$ and $2p_{1/2}$ which are centered at 642 and 653.8 eV, respectively, with a spin-energy separation of 11.8 eV are in good agreement with reported data of Mn $2p_{3/2}$ and Mn $2p_{1/2}$ in MnO_2 (Figure 2b).[34] Scanning electron microscopy (SEM) images of MnO_2/CNT hybrid nanostructures clearly shows uniform coaxial nanostructure (Figure 3). Electrodes are highly porous as revealed from SEM images of individual MnO_2 nanotubes and CNTs (see Supporting Information, Figures 1S and 2S). MnO_2 nanotube walls were found to be ~10 nm thick with good crystallinity and smooth surface. The structure of coaxial nanotubes such as MnO_2 shell thickness and nanotube length could be easily controlled by varying the infiltration time, which will enable us to tune the electrochemical properties of the coaxial nanotubes. CNTs protrude on both ends of the nanotubes, enabling an effective contact with the gold thin film current collector. Recently, coaxial nanowires of MnO_2/PEDOT have been synthesized by the coelectrodeposition method.[35] However,

in the present study, presence of a CNT core has superior advantages in terms of electrical conductivity, mechanical stability, and electrochemical performance. Also, high-temperature annealing results in high crystallinity of the coaxial nanostructure. The growth process of the coaxial nanotubes follows a typical template synthesis, wherein the manganese precursor initially combines with the template by impregnation and results in the nucleation and growth following annealing treatment. This forms the MnO_2 shell. The chemical vapor deposition process allows CNTs to grow in the inner cores left by the MnO_2 shells. Upon removal of templates, coaxial nanotubes with CNT core and MnO_2 shell are obtained.

Apart from fast Li insertion/deinsertion, high electronic conductivity of the electrode materials is necessary to develop high-performance lithium batteries. Electrochemical performance of MnO_2/CNT coaxial nanotubes as cathodes in Li batteries has been evaluated using galvanostatic charge−discharge measurements. Electrochemical performance of MnO_2 nanotubes and CNTs were also individually analyzed for comparison. Voltage versus specific capacity curves were obtained by cycling the cell at a constant rate of 50 mA/g between 3.2 and 0.02 V versus Li/Li^+ (Figure 4). A first discharge capacity of 2170 mA h/g and a reversible capacity of ~500 mA h/g after 15 cycles were observed for MnO_2/CNT hybrid coaxial nanotubes. Charge−discharge profiles of coaxial nanotubes are observed to be similar to that of MnO_2 tubes (see Supporting Information, Figure 3S and Figure 4S). A large irreversible capacity is observed, which could be due to drastic, lithium-driven, and structural or textural modifications, as observed for transition metal oxide electrodes.[10] The large irreversible capacity occurring only in the first cycle may be caused by decomposition reactions of the electrolyte and formation of the SEI (solid electrolyte interphase) film on the surface of the manganese oxide electrode.[36] A high reversible capacity observed for MnO_2/CNT hybrid coaxial nanotubes compared to MnO_2 nanotubes indicates reduced structural changes. The reaction mechanism of different materials with lithium varies as classical Li insertion/deinsertion in the case of carbon-based materials to Li-alloying processes in the case of metal/alloy. With reference to transition metal oxides, the reaction mechanism of manganese oxide with lithium has been proposed as[10]

$$MnO_2 + 4Li^+ + 4e^- \leftrightarrow 2Li_2O + Mn \qquad (1)$$

$$4Li \leftrightarrow 4Li^+ + 4e^- \qquad (2)$$

$$MnO_2 + 4Li \leftrightarrow 2Li_2O + Mn \qquad (3)$$

Hence, the process involves the formation and decomposition of Li_2O, accompanying the reduction and oxidation of metal nanoparticles. Extraction of lithium from Li_2O is extremely difficult and has been shown to be possible with the use of nanosized materials.[10,24] Bulk MnO_2 typically exhibited capacity no more than 120 mA h/g. Higher capacity values of the nanofibers over their bulk counterparts were proposed to be derived from the large surface areas of the nanosized materials. However, there has been an inconsistency in the electrochemical behavior of MnO_2 nanotubes, presumably due to the different mechanism between lithium insertion
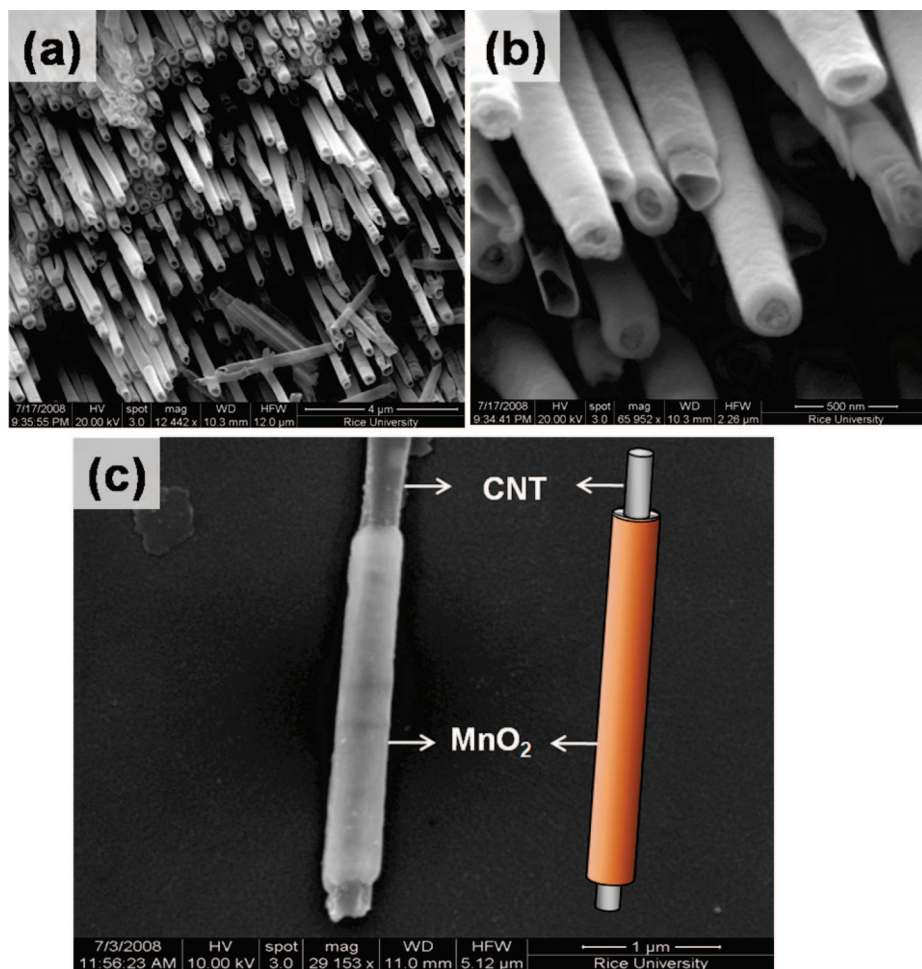
Figure 3. Textural characterization of MnO$_2$/CNT hybrid coaxial nanotubes. (a) Low- and (b) high-resolution SEM images showing the coaxial nature of the nanotube. (c) SEM image and a schematic representation of a single coaxial nanotube. The MnO$_2$ shell and carbon nanotube core are clearly seen.

and conversion reactions.[25] To understand the electrochemical mechanism of the reactions between manganese oxide electrode and lithium, XPS measurement has been applied to examine the valence change of manganese before and after lithium storage (Figure 2b,c). XPS spectra of MnO$_2$/CNT hybrid nanotubes after lithium storage (Figure 2c) shows broader peaks of Mn 2p binding energy compared to the pristine electrode, indicating the presence of metallic manganese resulted from the reduction of manganese oxide during lithiation process. XPS of the Li 1s peak centered at 55.3 eV confirms the formation of Li$_2$O (inset of Figure 2c). Formation of manganese metal and Li$_2$O during the initial lithiation process has been thus confirmed using XPS.

We expect that the use of coaxial nanotubes having two different Li storage mechanism has enhanced the total Li storage capacity. The nanosized and porous nature of the MnO$_2$ shell allows fast ion diffusion. In addition, the highly electrical conductive CNT core facilitates electron transport to the MnO$_2$ shell, which has low conductivity that can limit its charge/discharge rate. Moreover, presence of CNTs in the core of hybrid nanotubes will also act as additional lithium storage sites, leading to a dual mechanism of lithium storage and thereby resulting in an improved reversible capacity. Cyclic stability of CNTs and MnO$_2$ nanotubes has been compared with the MnO$_2$/CNT coaxial

nanotubes (Figure 4b). The MnO$_2$/CNT hybrid coaxial nanotube electrode resulted in an enhanced reversible specific capacity by an order compared to MnO$_2$ nanotubes, at the end of 15th cycle. Thus, improved performance of coaxial nanotube electrodes is attributed to improved conductivity by providing highly conductive CNTs in the inner core of the MnO$_2$ nanotubes, homogeneous electrochemical accessibility and high ionic conductivity by avoiding agglomerative binder, well-directed conductive paths due to perfect coaxial alignment, and a dual lithium storage mechanism of insertion/deinsertion in the case of CNTs and formation and decomposition of Li$_2$O in the case of MnO$_2$ nanotubes. We believe that porous structure of the electrodes decreases the effective diffusion path and increases the surface area for insertion and extraction of Li$^+$; meanwhile the CNT core acts as a buffer to alleviate the volume expansion caused by repeated ionic intercalation.

In summary, combination of simple vacuum infiltration and chemical vapor deposition techniques was used to prepare MnO$_2$/CNT hybrid coaxial nanotube arrays using porous alumina templates. The coaxial hybrid structure formed by the highly conductive CNT core offers enhanced electronic transport to the MnO$_2$ shell and acts as a buffer
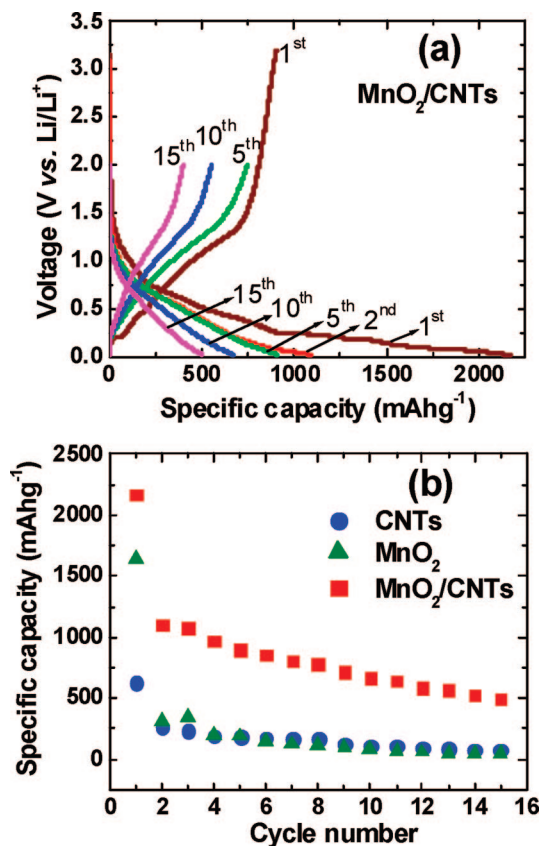
Figure 4. Electrochemical properties of MnO$_2$/CNT hybrid coaxial nanotubes as positive electrodes in Li battery. (a) Charge–discharge voltage profiles for MnO$_2$/CNT nanotube electrodes cycled at a rate of 50 mA/g between 3.2 and 0.02 V vs Li/Li$^+$. (b) Variation in discharge capacity vs cycle number for MnO$_2$/CNT nanotubes, MnO$_2$ nanotubes, and carbon nanotubes.

to alleviate the volume expansion. CNTs provide additional sites for lithium storage, resulting in dual mechanism of lithium storage, leading to an enhanced reversible capacity for MnO$_2$/CNT hybrid coaxial nanotubes by an order compared to template grown MnO$_2$ nanotubes.

Supporting Information Available: Descriptions of synthesis and characterization of nanotubes and electrochemical measurements and figures showing textural characterization of nanotubes, electrochemical charge-discharge voltage profiles, and voltage vs time profiles. This material is available free of charge via the Internet at http://pubs.acs.org.

References

(1) Arico, A. S.; Bruce, P.; Scrosati, B.; Tarascon, J. M.; Van Schalkwijk, W. *Nat. Mater.* **2005**, *4*, 366–377.

(2) Pushparaj, V. L.; Shaijumon, M. M.; Kumar, A.; Murugesan, S.; Ci, L.; Vajtai, R.; Linhardt, R. J.; Nalamasu, O.; Ajayan, P. M. *Proc. Natl. Acad. Sci. U.S.A.* **2007**, *104*, 13574–13577.

(3) Shaijumon, M. M.; Ou, F. S.; Ci, L.; Ajayan, P. M. *Chem. Commun.* **2008**, *20*, 2373–2375.

(4) Chan, C. K.; Peng, H.; Liu, G.; McIlwrath, K.; Zhang, X. F.; Huggins, R. A.; Cui, Y. *Nat. Nanotechnol.* **2008**, *3*, 31–35.

(5) Chung, S. Y.; Bloking, J. T.; Chiang, Y. M. *Nat. Mater.* **2002**, *1*, 123–128.

(6) Whittingham, M. S. *Chem. Rev.* **2004**, *104*, 4271–4301.

(7) Croce, F.; Appetecchi, G. B.; Persi, L.; Scrosati, B. *Nature* **1998**, *394*, 456–458.

(8) Thackeray, M. M. *Prog. Solid State Chem.* **1997**, *25*, 1–71.

(9) Jiao, F.; Bruce, P. G. *Adv. Mater.* **2007**, *19*, 657–660.

(10) Poizot, P.; Laruelle, S.; Grugeon, S.; Dupont, L.; Tarascon, J. M. *Nature* **2000**, *407*, 496–499.

(11) Badway, F.; Plitz, I.; Grugeon, S.; Laruelle, S.; Dolle, M.; Gozdz, A. S.; Tarascon, J. M. *Electrochem. Solid-State Lett.* **2002**, *5* (6), A115–A118.

(12) Nam, K. T.; Kim, D. W.; Yoo, P. J.; Chiang, C. Y.; Meethong, N.; Hammond, P. T.; Chiang, Y. M.; Belcher, A. M. *Science* **2006**, *312*, 885–888.

(13) Chan, C. K.; Peng, H.; Twesten, R. D.; Jarausch, K.; Zhang, X. F.; Cui, Y. *Nano Lett.* **2007**, *7*, 490–495.

(14) Dillon, A. C.; Mahan, A. H.; Deshpande, R.; Parilla, P. A.; Jones, K. M.; Lee, S. H. *Thin Solid Films* **2008**, *516*, 794–497.

(15) Subramanian, V.; Burke, W. W.; Zhu, H.; Wei, B. *J. Phys. Chem. C* **2008**, *112*, 4550–4556.

(16) Kavan, L.; Exnar, I.; Cech, J.; Graetzel, M. *Chem. Mater.* **2007**, *19* (19), 4716–4721.

(17) Badway, F.; Mansour, A. N.; Pereira, N.; Al-Sharab, J. F.; Cosandey, F.; Plitz, I.; Amatucci, G. G. *Chem. Mater.* **2007**, *19* (17), 4129–4141.

(18) Derrien, G.; Hassoun, J.; Panero, S.; Scrosati, B. *Adv. Mater.* **2007**, *19*, 2336–2340.

(19) Ng, S. H.; Wang, J.; Wexler, D.; Konstantinov, K.; Guo, Z. P.; Liu, H. K. *Angew. Chem., Int. Ed.* **2006**, *45*, 6896–6899.

(20) Thackeray, M. M.; Rossouw, M. H.; de Kock, A.; de la Harpe, A. P.; Gummow, R. J.; Pearce, K.; Liles, D. C. *J. Power Sources* **1993**, *434*, 289–300.

(21) Desilvestro, J.; Haas, O. *J. Electrochem. Soc.* **1990**, *137*, C5–C22.

(22) Sugantha, M.; Ramakrishnan, P. A.; Hermann, A. M.; Warmsingh, C. P.; Ginley, D. S. *Int. J. Hydrogen Energy* **2003**, *28*, 597–600.

(23) Kim, D. K.; Muralidharan, P.; Lee, H. W.; Ruffo, R.; Yang, Y.; Chan, C. K.; Peng, H.; Huggins, R. A.; Cui, Y. *Nano Lett.* **2008**, *8*, 3948–3952.

(24) Wu, M. S.; Chiang, P. C. J.; Lee, J. T.; Lin, J. C. *J. Phys. Chem. B* **2005**, *109*, 23279–23284.

(25) Cheng, F.; Tao, Z.; Liang, J.; Chen, J. *Chem. Mater.* **2008**, *20*, 667–681.

(26) Kim, D. W.; Hwang, I. S.; Kwon, S. J.; Kang, H. Y.; Park, K. S.; Choi, Y. J.; Choi, K. J.; Park, J. G. *Nano Lett.* **2007**, *7* (10), 3041–3045.

(27) Park, J. H.; Ko, J. M.; Park, O. O. *J. Electrochem. Soc.* **2003**, *150*, A864–A867.

(28) Reddy, A. L. M.; Ramaprabhu, S. *J. Phys. Chem. C* **2007**, *111* (21), 7727.

(29) Liao, S.; Holmes, K. A.; Tsaprailis, H.; Birss, V. I. *J. Am. Chem. Soc.* **2006**, *128* (11), 3504–3505.

(30) Reddy, A. L. M.; Ramaprabhu, S. *J. Phys. Chem. C* **2007**, *111* (44), 16138–16146.

(31) Shaijumon, M. M.; Rajalakshmi, N.; Ramaprabhu, S. *Appl. Phys. Lett.* **2006**, *88*, 253105.

(32) Rajalakshmi, N.; Ryu, H.; Shaijumon, M. M.; Ramaprabhu, S. *J. Power Sources* **2005**, *140* (3), 250–257.

(33) Chen, J.; Liu, Y.; Minett, A. I.; Lynam, C.; Wang, J.; Wallace, G. G. *Chem. Mater.* **2007**, *19*, 3595–3597.

(34) Liu, D.; Zhang, Q.; Xiao, P.; Garcia, B. B.; Guo, Q.; Champion, R.; Cao, G. *Chem. Mater.* **2008**, *20* (4), 1376–1380.

(35) Liu, R.; Lee, S. B. *J. Am. Chem. Soc.* **2008**, *130* (10), 2942–2943.

(36) Dedryvere, R.; Laruelle, S.; Grugeon, S.; Poizot, P.; Gonbeau, D.; Tarascon, J. M. *Chem. Mater.* **2004**, *16* (6), 1056–1061.

NL803081J